Check for updates

Exploring the optical properties of CuCo$_2$O$_4$-doped polyethylene oxide and carboxymethylcellulose for optoelectronic application

H. M. Ragab[1] · N. S. Diab[1] · Eshraga Abdallah Ali Elneim[1] · Noha H. El Fewaty[2] · Ahmed N. Al-Hakimi[3,4] · M. O. Farea[5]

Abstract

Nanocomposite films comprising polyethylene oxide (PEO) and carboxymethylcellulose (CMC) were fabricated via the solution casting process, with the incorporation of copper cobaltite nanoparticles (CuCo$_2$O$_4$ NPs). The study investigated the impact of CuCo$_2$O$_4$ NPs on the structural and optical properties of the PEO/CMC polymer blend, using X-ray diffraction, Fourier transform infrared (FTIR), and ultraviolet–visible spectroscopy (UV–Vis). The Debye–Scherrer equation was utilized to determine the size of the nanoparticles, and the results showed that the nanoparticle size decreased upon dispersion within the host matrix. The FTIR spectra of PEO/CMC blends revealed distinct vibrational spectral bands. These bands exhibited variations in their intensities, signifying interactions attributed to hydrogen bonds in the polymers. Various optical parameters, including energy gap, refractive index, Urbach energy, and extinction coefficient, were examined. The transmittance of the PEO/CMC blend exhibited a decrease from 88.6 to 18.8% following the dispersion of 3 wt% CuCo$_2$O$_4$ NPs. The optical analysis revealed an increase in the refractive index and a reduction in the optical band gap values, which reduced from 4.37 eV in the polymer blend to 3.77 eV in samples containing 3 wt% CuCo$_2$O$_4$. Furthermore, an increase in Urbach energy was observed with the rise in CuCo$_2$O$_4$ NPs content. The study also explored the influence of CuCo$_2$O$_4$ NPs on the fluorescence spectra of the PEO/CMC matrix and observed an increase in both optical dielectric and optical conductivity with increasing CuCo$_2$O$_4$ NPs content.

Keywords Polymer blend · Optical parameters · Energy gap · Refractive index · Urbach energy · Fluorescence

✉ H. M. Ragab
  ragab_200910@yahoo.com

1   Basic Sciences Department, Deanship of Preparatory Year, University of Ha'il, Hail, Saudi Arabia

2   Physics Department, Faculty of Science, Cairo University, Cairo 12613, Egypt

3   Department of Chemistry, College of Sciences, Qassim University, 51452 Buraidah, Qassim, Saudi Arabia

4   Department of Chemistry, Faculty of Sciences, Ibb University, Ibb, Yemen

5   Physics Department, Faculty of Science, Ibb University, Ibb, Yemen

1 Introduction

Incorporating inorganic nanomaterials such as nanosheets, nanowires, nanoplatelets, nanotubes, and nanoparticles into organic polymer matrices introduces novel materials with vast technological potential for the generation of optoelectronic devices (Davachi et al. 2019; Cha et al. 2019; Ahmed et al. 2023). Nanocomposite materials offer the advantage of merging the beneficial properties of both components, and the fine-tuning of their final properties is achievable by adjusting the concentration of these components inside the host polymer (Morsi et al. 2018; Soliman et al. 2023). Polymer composites that incorporate desirable optical properties are crucial for the advancement of materials used in optical communications, optical sensors, solar cells, polarizers, and energy storage devices (Nofal et al. 2021). The promise of polymer/inorganic nanocomposites in optoelectronic devices has spurred commercial interest in integrating inorganic nanoparticles into polymers. Nanofiller is commonly added to polymer blends to enhance their optical and electrical properties (El-Naggar et al. 2023).

The amalgamation of multiple polymers has garnered considerable interest from numerous researchers owing to the emergence of distinctive properties (Heiba, et al. 2017, 2021; Heiba and Mohamed 2019). This method serves as a valuable approach for producing adaptable polymeric matrices characterized by a pronounced degree of compatibility (Heiba et al. 2022; Mohamed et al. 2018). Amidst these various polymers, Polyethylene oxide (PEO) and Carboxymethyl cellulose (CMC). PEO possesses a linear structure and exhibits a semi-crystalline nature, comprising both crystalline and amorphous phases at room temperature. However, in its pure form, PEO demonstrates a crystalline structure. Consequently, PEO has found extensive application as a foundational material in various polymer electrolyte systems (Kumar et al. 2012). Carboxymethyl cellulose (CMC), a biodegradable and non-toxic natural polymer, is a valuable component in the blending method due to its amorphous nature. This characteristic aids in increasing the amorphous content within PEO. Furthermore, CMC's anionic water-solubility helps minimize phase separation during blending, as it can interact with the host matrix through hydrogen bond creation via its OH groups. These intriguing properties make CMC versatile for various applications, including papermaking, printing, toiletries, food packaging, electrical components, and pharmaceuticals (El-Sayed et al. 2011; El-Bana et al. 2018). Rajeh et al. prepared different weight percentages of the PEO/CMC blend, where the theoretical interactions were introduced by the density functional theory (DFT). Furthermore, they found that the PEO/CMC blend (70/30 wt%) was more miscible and introduced high thermal stability and enhanced electrical conductivity as compared to the other weights of PEO/CMC blends (Rajeh and Morsi 2019).

The exploration of polymer/metal hybrid nanocomposites has gained growing significance due to the pivotal role that processability, functionality, and nanostructure size play in the development of electroactive polymers (Reddy et al. 2016). The integration of nanoceramic materials into the host materials has garnered significant interest due to its ability to introduce novel materials with enhanced physical and chemical properties. Consequently, these nanocomposites find versatile applications across various fields. Transition metals like cobaltite, exemplified by $CuCo_2O_4$, play a vital role as key components in numerous applications (Heiba et al. 2021). $CuCo_2O_4$, characterized by the common formula $Cu_xCo_{3-x}O_4$, is a noteworthy cobalt-containing spinel oxide that shows great promise as an electrode material for various applications, including hybrid supercapacitors, electrocatalysts, and Li-ion batteries. Its attractiveness stems from its cost-effectiveness, favorable

electrical characteristics, and outstanding electrochemical performance (Wang et al. 2015). In the case of CuCo$_2$O$_4$, two distinct direct band gaps (1.43 and 2.05 eV) were identified in thin film form (Liu et al. 2022). In contrast, when CuCo$_2$O$_4$ is synthesized using a one-step chemical route, a single optical band gap (4.02 eV) is observed (Koninck et al. 2006). CuCo$_2$O$_4$ typically demonstrates superior electrochemical performance in comparison to single metal oxides like Co$_3$O$_4$ and CuO. This superiority can be attributed to the presence of cobalt cations, which enhance electrochemical efficiency, copper cations that promote electrical conductivity, and the relatively low activation energy required for electron transport between the various metal constituents (Kaverlavani et al. 2017). This study is focused on improving the optical properties and electrical conductivity of the PEO/CMC blend (70/30 wt%) by incorporating varying levels of CuCo$_2$O$_4$ nanoparticles (NPs). Remarkably, there is a lack of prior research investigating the impact of CuCo$_2$O$_4$ NPs on the PEO/CMC blend, making this work pioneering in its approach. Additionally, this research encompasses a comprehensive analysis of the morphological, optical, and electrical properties of these nanocomposite films, utilizing appropriate analytical techniques.

2 Experimental

2.1 Chemicals

The PEO powder, which had a molecular weight of 35,000 g/mol, was obtained from ACROS Organic, located in Morris Plains, New Jersey. On the other hand, the CMC, with a molecular weight of 190,000 g/mol, was procured from BDH Chemical Ltd. in Poole, the United Kingdom. The CuCo$_2$O$_4$ material, supplied by Sigma-Aldrich in Germany, boasted an exceptional purity level of 99.998%. During the study, these chemicals were effectively dissolved in double distilled water (DDW).

2.2 Preparation of PEO/CMC-CuCo$_2$O$_4$ nanocomposite

PEO/CMC membranes, enriched with CuCo$_2$O$_4$ nanoparticles, were manufactured using a solution casting method. The process commenced with the preparation of a PEO solution, achieved by dissolving 0.7 g of PEO powder in 75 ml of double-distilled water (DDW). This mixture underwent magnetic stirring at 700 rpm and room temperature (RT) for an hour, ensuring complete powder dissolution. Subsequently, a CMC solution was formed by dissolving 0.3 g of CMC in 75 ml of DDW, followed by its combination with the desired amount of PEO. Magnetic stirring at 700 rpm and RT continued for an additional hour until a homogeneous solution was obtained. To generate CuCo$_2$O$_4$ filler dispersions with concentrations of 5%, 10%, and 15% by weight, distinct quantities of CuCo$_2$O$_4$ were suspended in 20 ml of DDW, supplemented with a 1% acetic acid solution. These CuCo$_2$O$_4$ dispersions were then individually integrated into the PEO/CMC solutions while maintaining continuous stirring. The resulting mixtures were uniform. Then, the homogenous solutions were cast into clean, dry Petri dishes and underwent a vacuum drying process at 50 °C for two days, facilitating the development of solvent-free films. The nanocomposite films exhibited thicknesses ranging from 75 to 87 μm. The samples were coded as S0, S1, S2, and S3, representing PEO/CMC composites with 0%, 1.0%, 2.0%, and 3.0% by weight of CuCo$_2$O$_4$ nanofiller, respectively.

2.3 Characterizations

Various analytical techniques were employed to assess the properties of PEO/CMC composites and PEO/CMC-CuCo$_2$O$_4$ nanocomposites: 1-X-ray Diffraction (XRD): XRD with a Diano XRD 800 diffractometer was used to examine the crystalline structure of the materials. 2- Fourier Transform Infrared (FT-IR) Spectroscopy: FT-IR spectroscopy using a Nicolet iS10 instrument helped identify functional groups within the nanocomposite films. 3- The optical properties were studied by a diffused reflectance spectroscopy JASCO (V-570) 4- Broadband Dielectric Measurements: Broadband dielectric measurements were conducted in a dry nitrogen environment using the Novo Control Turnkey Concept 40 System to examine the electrical properties and conductance behavior of the materials at different frequencies. These analyses provided a comprehensive understanding of the structural, chemical, optical, and electrical characteristics of the composites, offering valuable insights for further research and potential applications.

3 Results and discussion

3.1 XRD analysis

XRD investigations play a pivotal role in elucidating microstructural changes in polymeric materials. In this context, XRD was utilized to discern whether the PEO/CMC-CuCo$_2$O$_4$ NPs polymer nanocomposite samples exhibit amorphous or crystalline regions and to assess how CuCo$_2$O$_4$ NPs influence the structural properties of the polymer nanocomposites. Figure 1 displays the XRD pattern of CuCo$_2$O$_4$ nanoparticles. The X-ray diffractograms of the CuCo2O4 powders reveal distinct reflection peaks at $2\theta = 18.87°$, $31.18°$, $36.73°$, $38.54°$, $44.69°$, $55.49°$, $59.12°$, and $64.96°$. These diffraction peaks exhibit a strong correspondence with the (111), (220), (311), (222), (400), (331), (422), and (333) crystal
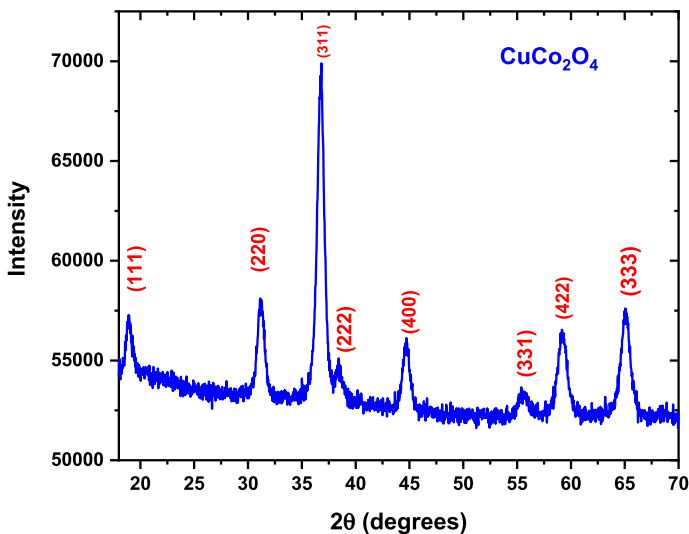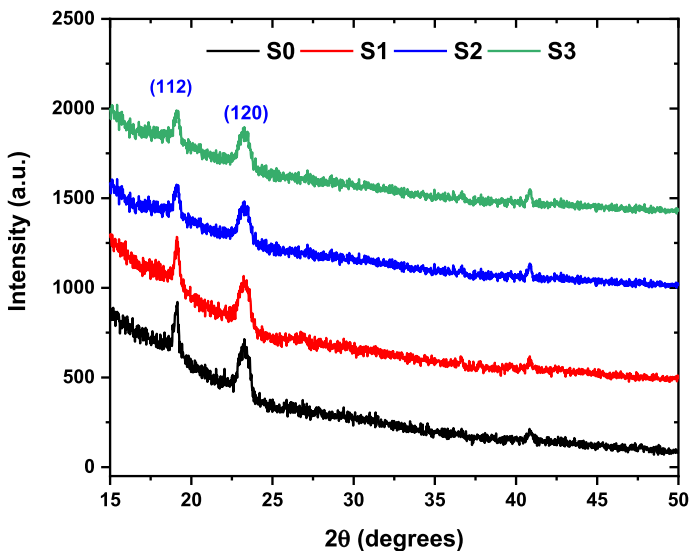

Fig. 1 XRD pattern of CuCo$_2$O$_4$ nanoparticles

planes of a cubic spinel copper cobaltite. Notably, the positions of these diffraction peaks align closely with the data provided in the ICDD cards for pristine $CuCo_2O_4$ (JCPDS− ICDD 1-1155 file) (Flores-Lasluisa et al. 2019). In Fig. 2, the XRD diffraction patterns illustrate the characteristics of the PEO/CMC and the PEO/CMC incorporated with different concentrations of $CuCo_2O_4$ nanoparticles. Specifically, the XRD curve of the virgin PEO/CMC reveals its semicrystalline nature, attributed to the existence of the semicrystalline PEO, and exhibits two distinct and sharp peaks at 19.12° and 23.26°. These peaks correspond to crystallographic planes (112) and (120) [PCPDF File numbers 49-2203 and 49-2202] (Ragab et al. 2016; Abdelghany et al. 2016). Furthermore, the XRD curve of the S0 reveals several low-intensity peaks at $2\theta = 26.85°$, 36.70°, and 40.84°. When examining the XRD patterns of the fabricated films with the inclusion of $CuCo_2O_4$ nanoparticles, a slight reduction in the intensity of the sharp peaks (at 19.12° and 23.26°) observed in the PEO/CMC composite is evident, implying a decrease in the crystalline content within the PEO/CMC composite. Upon a comparison of the XRD patterns of $CuCo_2O_4$ NPs and the polymer nanocomposites loaded with $CuCo_2O_4$ NPs at concentrations of 1.0, 2.0, and 3 wt%, no discernible diffraction peaks corresponding to the lattice planes of $CuCo_2O_4$ NPs are observed within the polymer nanocomposites. This outcome could be attributed to either the limited $CuCo_2O_4$ NPs content, which does not exceed 3%, or the possibility of $CuCo_2O_4$ NPs being encapsulated within the polymeric matrix.

The calculation of the average crystallite size was performed using the Scherrer equation, which is expressed by the following formula (Albalawi et al. 2023):

$$D = \frac{0.9\lambda}{\beta \cos \theta} \tag{1}$$

Here, θ symbolizes Bragg's angle, D represents the full width at half maximum of the diffraction peak, and λ corresponds to the X-ray wavelength of the XRD machine (with a value of $\lambda = 0.15405$ nm). It's important to note that the diffraction peaks observed in the

Fig. 2 XRD patterns of pure PEO/CMC polymer and PEO/CMC doped with various filling levels of $CuCo_2O_4$ nanoparticles

XRD patterns of the polymer nanocomposites (PNC) films were associated with the PEO/CMC blend. The crystallinity degree (X_{dc}%) was calculated using the Hermans–Weidinger method (Hermans and Weidinger 1949):

$$X_{dc} = \frac{area\ under\ crystlline\ peaks}{total\ area\ under\ all\ peaks} \times 100 \qquad (2)$$

Table 1 provides the calculated X_{dc}% values for the PEO/CMC-CuCo$_2$O$_4$ NPs nanocomposite films. The alteration in the crystalline structure can be attributed to the influence of CuCo$_2$O$_4$ NPs on the composition of the PEO/CMC polymeric matrix. This outcome suggests that the addition of CuCo$_2$O$_4$ NPs, which possess strong crystalline properties, to the PEO/CMC blend, can physically augment the amorphous regions within the polymer blend, thereby reducing its semi-crystalline nature. This reduction in semi-crystallinity may indicate a chemical effect, signifying an increase in disorder due to a reduction in the number of intermolecular bonds inside the polymeric matrix. The decrease in the crystalline structure could potentially result in heightened ionic mobility, subsequently leading to increased electrical conductivity. This enhancement could prove beneficial in various applications, particularly in energy storage devices.

3.2 FTIR spectroscopy

FT-IR spectroscopy serves as a valuable tool for elucidating intermolecular interactions among the components within the polymeric matrix (Rajeh et al. 2019). Figure 3 illustrates the FTIR absorption spectra for the PEO/CMC composite and the PEO/CMC containing varying quantities of CuCo$_2$O$_4$ NPs. As observed in Fig. 3, all the spectra of the prepared samples exhibit the primary functional groups characteristic of the pristine polymer. These comprise the following vibrational modes: OH stretching of CMC, CH$_2$ asymmetric stretching, COO-stretching of CMC, and C–O–C stretching of PEO. Analysis of the PEO/CMC spectra reveals a significant increase in absorbance for the characteristic peaks of PEO/CMC at 887, 712, and 598 cm^{-1} in the PEO/CMC-1.0 wt% CuCo$_2$O$_4$ NPs. As the concentration of CuCo$_2$O$_4$ inside the polymeric chain increases, the intensity of these functional groups diminishes significantly, eventually disappearing entirely in the spectrum of the final sample. This behavior is consistent for functional groups observed at 3338, 2919, 1578, 1403, 1313, and 1020 cm^{-1}. CMC demonstrates a significant propensity to establish intermolecular hydrogen bonds when interacting with polymers that feature highly electronegative groups within their structures (Gupta et al. 2013). Moreover, polymers that incorporate electronegative oxygen, like PEO polymers, are adept at accepting protons due to the abundance of these functional groups (Abdelrazek et al. 2018). Consequently,

Table 1 The values of energy gap (direct and indirect), crystalline degree (X_{dc} %), Urbach energy (E_u), and refractive index (n) for nanocomposite samples under investigation

Samples	CuCo$_2$O$_4$ (wt%)	E_g direct	E_g indirect	X_{dc}	n ($\lambda=550$ nm)	E_u (eV)
S0	0.0	5.54	4.37	25.13	1.515	0.21
S1	1.0	5.37	4.15	22.32	2.221	0.24
S2	2.0	5.20	4.01	18.22	2.632	0.25
S3	3.0	4.95	3.77	14.46	3.105	0.42
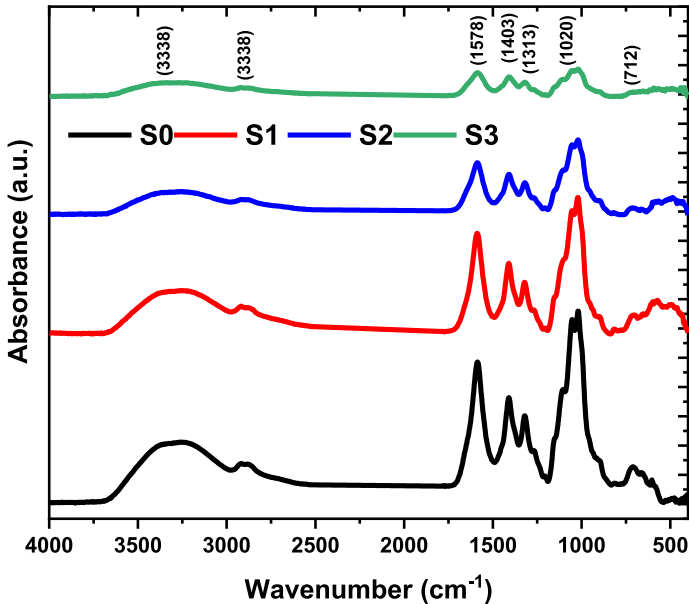
Fig. 3 FT-IR spectra of PEO/CMC polymer and PEO/CMC doped with different filling levels of CuCo$_2$O$_4$ nanoparticles

the prevailing heterochain interaction primarily involves the formation of hydrogen bonds between the functional groups of the polymer blend and the CuCo$_2$O$_4$ nanoparticles.

3.3 Optical parameters

3.3.1 Absorption, transmission, and reflection spectra

Figure 4 illustrates the UV–visible absorption spectra of PEO/CMC composite and PEO/CMC filled with different filling levels of CuCo$_2$O$_4$ nanoparticles. Evident in the absorption spectra of the PEO/CMC blend is a distinct absorption edge, indicating the semicrystalline structure of this polymeric material (Ebnalwaled and Thabet 2016). Similarly, with an increase in the concentration of CuCo$_2$O$_4$ nanoparticles within the polymeric matrix, there was an observed red shift in the absorption edge. This phenomenon could potentially be attributed to the enlargement of copper cobaltite particle size within the polymer matrix (Khordad 2016). The absorption edge, characterized by a pronounced decrease in intensity within the wavelength range of $233 < \lambda < 260$ nm, shifted towards longer wavelengths, indicating a decrease in photon energy. This shift suggests a decrease in the energy gap as the concentration of fillers within the polymeric matrix increases (Soliman and Vshivkov 2019). Figure 5 displays the optical transmission spectra of the polymer blend (PEO/CMC) infused with different quantities of CuCo$_2$O$_4$ nanoparticles as fillers. Notably, the prepared samples exhibit minimal absorption within the 400 to 800 nm wavelength range. However, a decline in transmission becomes evident within the UV region (248–355 nm) due to a sharp absorption, which can be attributed to the enlargement of copper cobaltite particle size within the polymer matrix (Soliman and Vshivkov 2019). Furthermore, as the
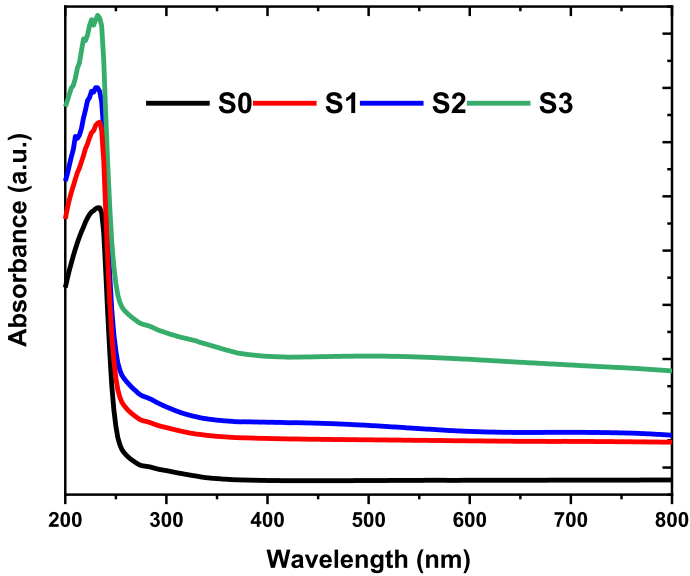
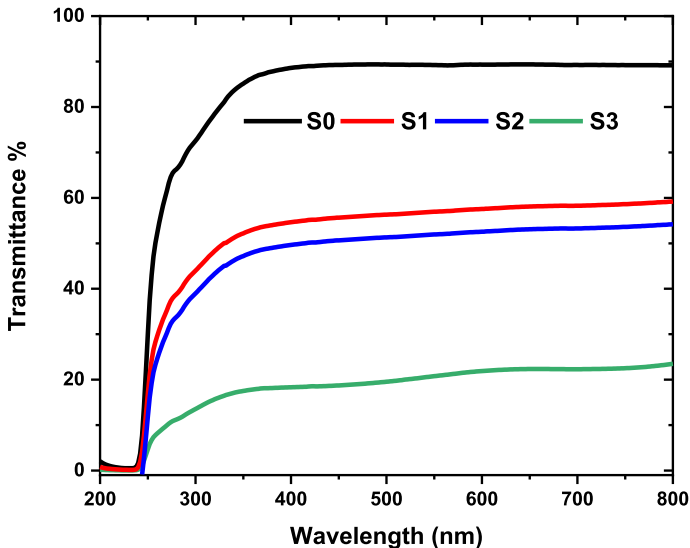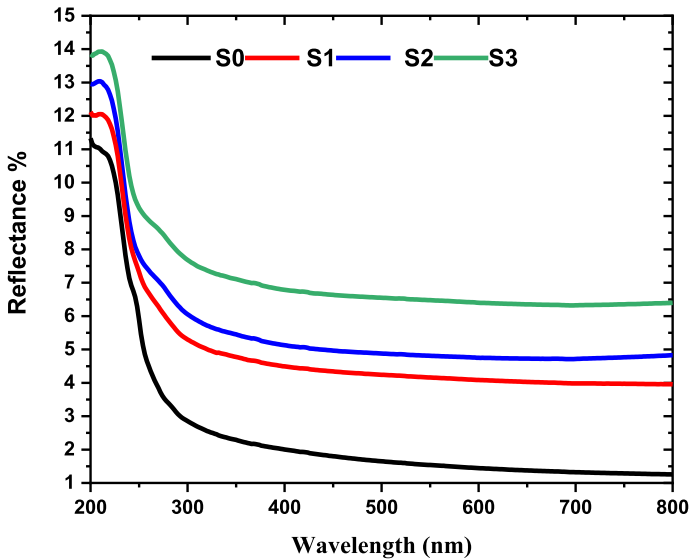**Fig. 4** UV–Vis absorption spectra for PEO/CMC/CuCo$_2$O$_4$ nanocomposite samples

Fig. 5 Transmittance spectra versus wavelength for PEO/CMC/CuCo$_2$O$_4$ nanocomposite samples

concentration of copper cobaltite nanoparticles in the polymeric matrix increases, there is a concurrent decrease in transmittance. Specifically, the PEO/CMC polymer blend exhibits the highest optical transmission, reaching approximately 88.6%. However, this transmission diminishes significantly to approximately 18.8% for the nanocomposite containing 3 wt% copper cobaltite nanoparticles, with this reduction occurring at a wavelength of approximately 409 nm. Figure 6 illustrates the wavelength-dependent reflectance spectrum

Fig. 6 Reflection spectra versus wavelength for $PEO/CMC/CuCo_2O_4$ nanocomposite samples

of the polymer blend (PEO/CMC) containing various concentrations of $CuCo_2O_4$ nanoparticles as a nanofiller. Notably, the reflectance shows a rising trend with an increase in $CuCo_2O_4$ content. The blend of excellent transmittance and minimal reflectance highlights that these prepared films are well-suited as eco-friendly transparent packaging materials, especially for a broad spectrum of microelectronic and optoelectronic devices necessitating exceptionally clear external surfaces. These materials hold promise for use in diverse optical applications, such as broadband polymeric materials for diode lasers and other optical devices with stringent transparency requirements.

3.3.2 Optical energy gap (E_g) and Urbach energy (E_u)

The study of the dependence of the optical absorption coefficient on photon energy aimed to unveil information regarding the band structure and electron transition types present in the prepared films. This analysis was conducted using Tauc's power law (Alsalmah et al. 2023):

$$(\alpha h v) = C(h v - E_g)^r \tag{3}$$

Here the absorption coefficient (α) is computed by the formula $\alpha = 2.303 \times$ (absorbance/thickness), "hv" represents the energy of the incident photon, "C" represents a constant, "E_g" corresponds to the energy gap of the nanocomposite. The power "r" varies based on the nature of the transition. Specifically, "r" can take on values of ½ for direct transition or 2 for indirect transition. The determination of the direct energy gap involved employing a least squares fitting method based on the linear section of the $(\alpha h v)^2$ versus $(h v)$ plot, as depicted in Fig. 7a. Conversely, the indirect energy gaps were obtained through a similar fitting procedure using the linear portion of the $(\alpha h v)^{1/2}$ versus $(h v)$ plot, as depicted in
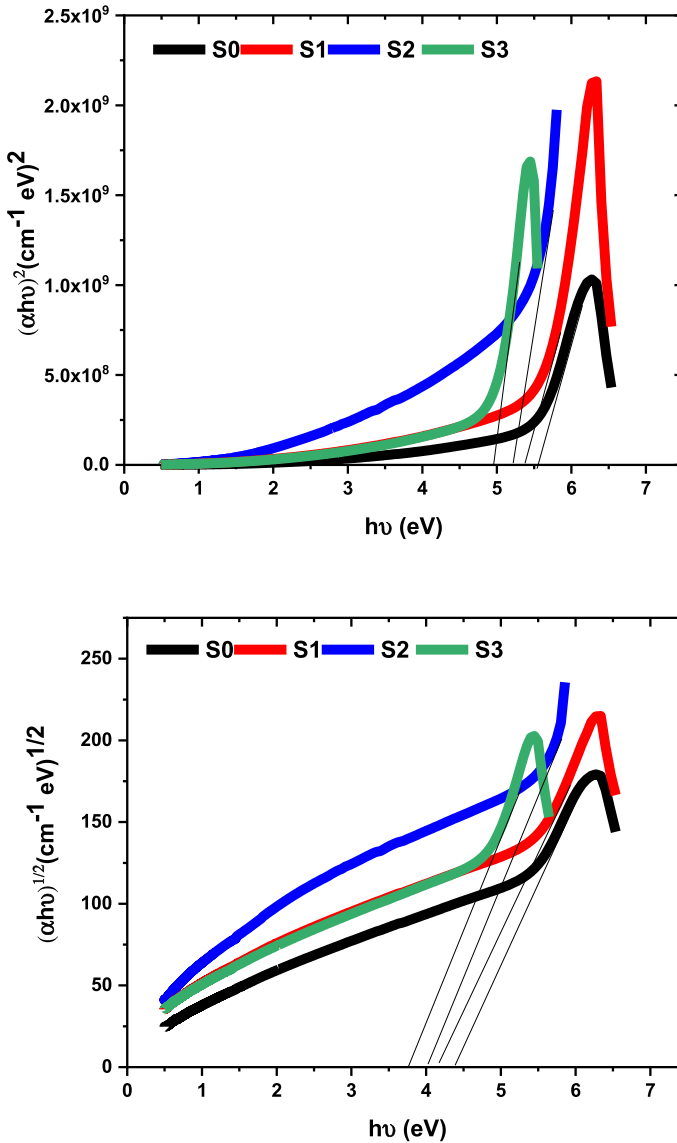
Fig. 7 The dependence of **a** $(\alpha h\upsilon)^2$ **b** $(\alpha h\upsilon)^{1/2}$ on $(h\upsilon)$ for PEO/CMC/CuCo$_2$O$_4$ nanocomposite samples

Fig. 7b. Direct and indirect transition energy gap values were extracted for the prepared nanocomposite films, and these values are listed in Table 1.

In Table 1, it is observed that the energy gap for PEO/CMC is 5.54, which decreases to 4.95 when incorporating 3 wt% of CuCo$_2$O$_4$ nanoparticles (NPs). These findings are consistent with our prior research (Alhagri et al. 2023), where a PEO/CMC-TiO$_2$ nanocomposite exhibited a similar trend. In that case, the energy gap for PEO/CMC was 5.46 and decreased to 3.45 when filled with 0.8 wt% TiO$_2$. This reduction in the energy gap is in accordance with the results obtained by El-naggar et al. (2022a) which, indicates structural

changes within the polymeric materials and is related to the formation of localized states within the band gap (El-Naggar et al. 2022; Heiba et al. 2020).

The optical transitions occur because of the existence of photons with energies (hυ) that fall below the optical band gap (E_g) of the material. This absorption of photons is associated with the presence of localized tail states within the forbidden gap (Sheha et al. 2012). The width of this tail, commonly referred to as the Urbach tail, offers valuable information about defect levels and serves as an indicator of the extent of disorder within the forbidden gap of the polymeric materials. The calculation of the Urbach tail width can be performed using the following equation (Sheha et al. 2012; Sharma and Aggarwal 2018):

$$\alpha = \alpha_o \exp\left(\frac{h\upsilon}{Eu}\right) \tag{4}$$

Here, α and $h\upsilon$ were defined in Eq. 3. The α_o represents a constant and E_u signifies the Urbach energy. The Urbach energy values can be derived by plotting the linear segment of (ln α) against (hυ), as demonstrated in Fig. 8. The reciprocal of the slope in this graph provides the Urbach energy values. These values are presented in Table 1. Significantly, the Urbach energy values exhibit an increase as the quantity of CuCo₂O₄ NPs is augmented. This increase indicates a higher density of localized tail states and suggests the occurrence of transition between these tail states (Taha et al. 2019).

3.3.3 Extinction coefficient (K) and refractive index (n)

The essential parameters for optical applications encompass the extinction coefficient (k) and the refractive index (n). These optical characteristics were computed using the reflectance and absorption coefficients (α), following the equations below (El-Naggar et al. 2021, 2022b):
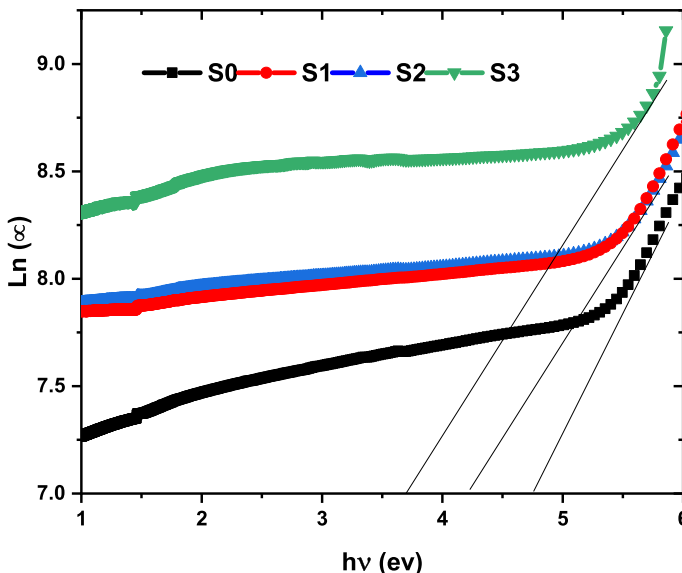

Fig. 8 Urbach plots for PEO/CMC/CuCo₂O₄ nanocomposite samples

$$n = \frac{1+R}{1-R}\sqrt{\frac{4R}{(1-R)^2}} - K^2 \qquad (6)$$

$$K = \frac{\alpha\lambda}{4n} \qquad (5)$$

$$\alpha(\lambda) = 2.303\frac{A}{d} \qquad (7)$$

Here, "R" represents reflectance, and "A" corresponds to absorption values. Figure 9 illustrates the variation of the extinction coefficient concerning the wavelength of incident light. The role of the extinction coefficient is to indicate the energy dissipation caused by scattering or absorption due to molecules and particles present within the materials. The extinction coefficient (K) increases with a higher concentration of $CuCo_2O_4$ NPs. In Fig. 9, at lower wavelengths within the range of 233 to 273 nm, the extinction coefficient exhibits a decrease. This behavior can be attributed to incident photons having sufficient energy to excite electrons from their initial states to higher energy states, resulting in reduced energy loss and, consequently, a lower extinction coefficient. Conversely, at higher wavelengths in the range of 300 to 800 nm, the extinction coefficient sharply rises. In this case, incident photons lack the energy required to excite electrons, leading to a substantial loss of energy and, consequently, a significant increase in the extinction coefficient. These findings align with previously reported data (Aziz et al. 2013; El-Naggar et al. 2022c; Heiba and Mohamed 2020).

Figure 10 displays the changes in the refractive index (n) with wavelength (λ) for the PEO/CMC-$CuCo_2O_4$ nanocomposite samples. The refractive index values increase as the concentration of $CuCo_2O_4$ NPs in the polymeric matrix increases. This increase is attributed to the higher packing density of $CuCo_2O_4$ NPs within the composite material (Abdul Nabi et al. 2014). As the concentration of $CuCo_2O_4$ NPs in the PEO/CMC blend increases,
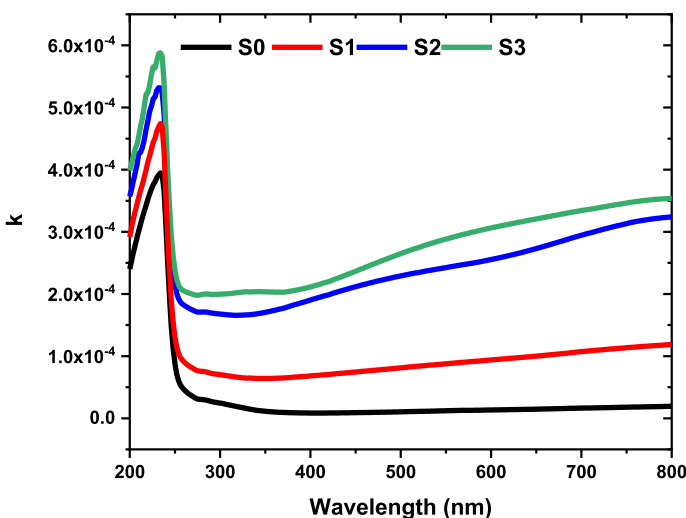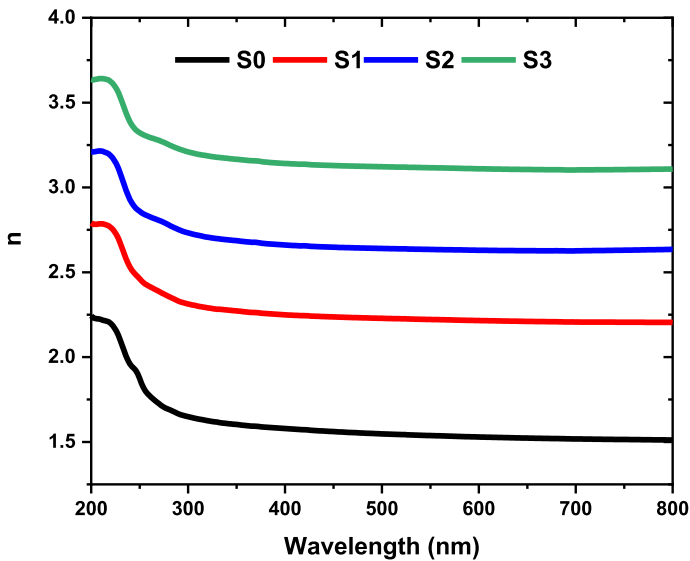

**Fig. 9** Extinction coefficient spectra versus (λ) for PEO/CMC/$CuCo_2O_4$ nanocomposite samples

Fig. 10 Refractive index (n) versus (λ) for PEO/CMC/CuCo$_2$O$_4$ nanocomposite samples

the refractive index undergoes a substantial transformation, rising from 1.515 to 3.105 (at λ = 550 nm). The refractive index (n) values are listed in Table 1. Figure 10 illustrates that the refractive index experiences a sharp decline as wavelength increases within the visible region, until reaching λ = 550 nm, after which it remains relatively constant in the 500 to 800 nm range. This rise in refractive index with an increasing concentration of CuCo$_2$O$_4$ NPs is a consequence of the interaction between incident light and the CuCo$_2$O$_4$ NP-doped polymeric matrix. This interaction results in heightened light refraction, leading to an overall increase in the refractivity of the composite samples (Sayed and Morsi 2014).

3.4 Fluorescence analysis

Figure 11 displays the fluorescence (FL) spectra of the PEO/CMC blend with varying quantities of CuCo$_2$O$_4$ nanoparticles, The FL spectrum of the PEO/CMC exhibits a broad wavelength range, spanning from 320 to 600 nm. Within this spectrum, sub-peaks corresponding to UV-violet (343, 417 nm), blue (437 nm), and yellow (571 nm) colors are discernible. The 571 nm sub-peak can be attributed to the π→π^* transition of PEO carbonyl groups (Kara et al. 2020). UV and violet emissions, linked to excitonic transitions, are associated with near-band emission (NBE) electron processes, while blue luminescence results from defects (Heiba et al. 2016). Xiong et al. (2001) observed that PEO, which is typically non-fluorescent, emits fluorescence when excited at 400 nm, manifesting three excitation peaks (at about 270, 325, and 370 nm) in the UV range and an emission peak at approximately 415 nm. This fluorescence in unmodified polymer materials may stem from trace fluorescent impurities. Furthermore, interactions between the primary and side chains of PEO and CMC can alter luminescence efficiency and spectral positioning. In non-fluorescent polymers, discrete chromophores, referred to as "sub-fluorophores," may undergo space conjugation via cooperative intramolecular conformation and intermolecular
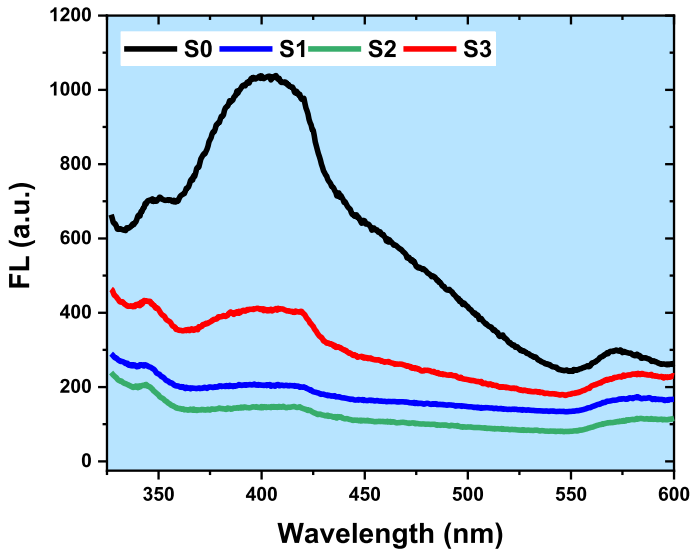
Fig. 11 FL data for PEO/CMC polymer blend and PEO/CMC filled with various filling levels of $CuCo_2O_4$ nanoparticles

aggregation, thereby leading to fluorescence or, on occasion, phosphorescence emissions (Chatterjee et al. 2020). The FL intensity diminishes upon loading $CuCo_2O_4$ into the PEO/CMC matrix, and this reduction becomes more pronounced as the $CuCo_2O_4$ quantity within the host matrix increases. This quenching effect may be attributed to the strong interaction between PEO/CMC and $CuCo_2O_4$, which generates trap sites through which excited electrons can be transferred (Li 2019). These studied doped blends hold potential for use in photocatalytic reactions.

3.5 Optical conductivity and optical dielectric properties

Regarding the measurement of dielectric parameters, it's important to note that these cannot be directly determined through spectrophotometer experiments. However, it is possible to calculate them using the following equations based on data for refractive index and extinction coefficients (Dadashi et al. 2015):

$$\varepsilon' = n^2 - k^2 \tag{8}$$

$$\varepsilon'' = 2nk \tag{9}$$

Here, ε' is the optical dielectric constant, and ε'' is the optical dielectric loss. Figure 12a, b illustrates the variations in ε' and ε'' as a function of $h\upsilon$. It is evident from Fig. 12 that both ε' and ε'' exhibit an upward trend in response to the increasing concentration of $CuCo_2O_4$ nanoparticles within the PEO/CMC blend. Notably, the ε' value surpasses that of ε''. This discrepancy can be attributed to their distinct dependencies on k, as outlined in Eqs. 8 and 9, coupled with the relatively low value of k, as indicated in Fig. 9. Furthermore, the augmentation of the optical dielectric constant with rising photon energy can be attributed to the interactions between photons and electrons within
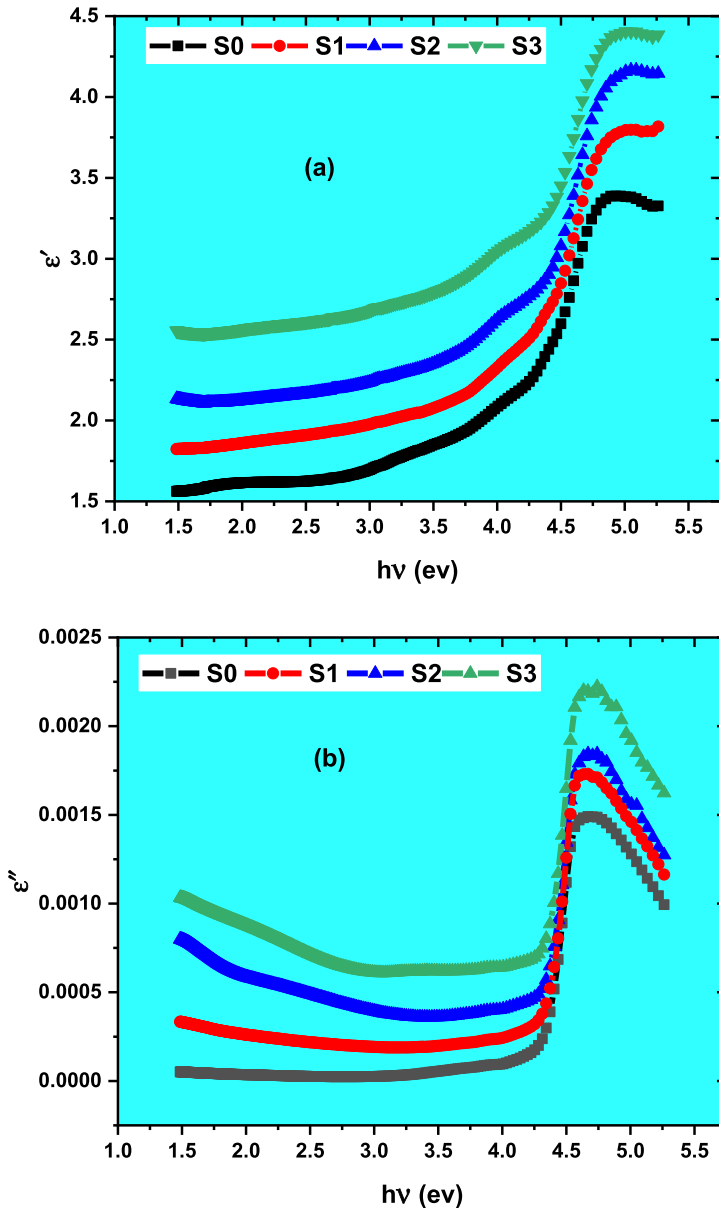
Fig. 12 **a** Optical dielectric constant ε' and **b** optical dielectric loss ε'' versus (hυ) for PEO/CMC/CuCo$_2$O$_4$ nanocomposites samples

the polymeric materials (Ebnalwaled and Thabet 2016). Beyond the ε' and ε'' values, the optical properties encompass a significant parameter known as optical conductivity, denoted as σ$_{opt}$. This parameter describes how the material responds to the movement of charge carriers induced by the excitation caused by incident photon energy (Taha and Saleh 2018). The following equation explains how the refractive index and absorption

coefficient of the materials directly affect optical conductivity (Taha and Saleh 2018; Abutalib and Yahia 2019):

$$\sigma_{opt} = \frac{n\alpha C}{4\pi} \tag{10}$$

Here, C represents the light speed. The relationship between (σ_{opt}) and (hυ) for various quantities of $CuCo_2O_4$ nanoparticles is presented in Fig. 13. It is evident that in general, optical conductivity (σ_{opt}) increases with rising photon energy (hυ). This trend can be categorized into two distinct regions. In the low photon energy area (hυ < 4 eV), the incident photon energy is unable to excite electrons within the polymeric matrix. Consequently, optical conductivity appears to remain relatively constant within this range. However, as we enter the high photon energy region (hυ > 4 eV), the energy levels of the incident photons become adequate to excite electrons from the valence band to the conduction band. This results in an increase in the population of charge carriers and, consequently, an increase in optical conductivity. It is worth noting that the creation of localized tail states within the band gap facilitates the transitions from the valence band to nearby energy states, contributing to this phenomenon. Furthermore, a decline in the polymer films' crystallinity degree results in a decrease in the energy gap and a simultaneous rise in the optical conductivity (Mohamed and Abdel-Kader 2019).

4 Conclusion

The study focused on examining the structural and linear optical characteristics of pristine PEO/CMC and PEO/CMC composites enhanced with $CuCo_2O_4$ nanoparticles. The XRD analysis revealed that as the content of $CuCo_2O_4$ NPs increased, the crystallinity of the polymer nanocomposite films decreased. Additionally, FTIR absorption spectra indicated a

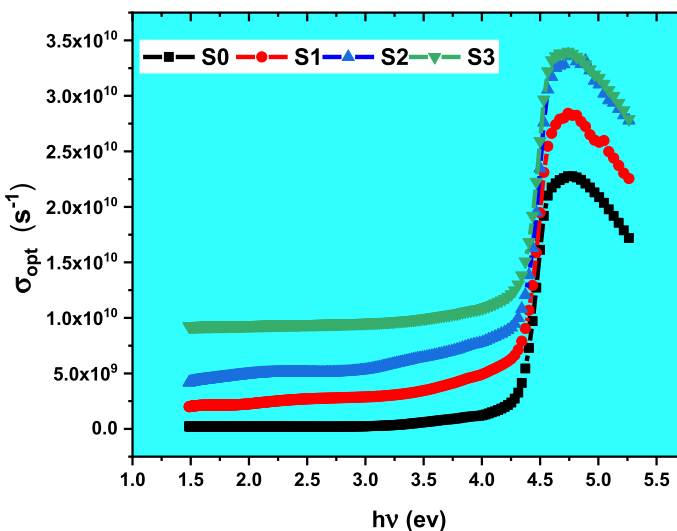**Fig. 13** Optical conductivity (σopt) versus (hυ) for PEO/CMC/CuCo₂O₄ nanocomposite samples

decrease in the absorbance of functional groups within the blends due to the incorporation of nanofillers, suggesting interaction between these groups and $CuCo_2O_4$ NPs. The investigation into optical properties involved analyzing absorbance, transmittance, and reflectance spectra. The energy gap values were decreased from 5.54 to 4.95 eV in the case of direct transition and decreased from 4.37 to 3.77 eV in the case of indirect transition, implying the semiconducting nature of the resulting nanocomposite samples. Furthermore, the Urbach energy increased from 0.21 to 0.42 eV with increasing $CuCo_2O_4$ NPs content, indicating a high density of localized tail states. The prepared samples displayed a significantly higher refractive index of n (PEO/CMC-3 wt% $CuCo_2O_4$ NPs) = 3.105, approximately twice as high as the refractive index of PEO/CMC n (PEO/CMC) = 1.515. Additionally, the optical dielectric properties and optical conductivity of the nanocomposite increased with higher $CuCo_2O_4$ NPs content in the host matrix. In conclusion, these samples, with adjustable energy gap, high refractive index, and relatively low $CuCo_2O_4$ NPs content, hold potential for applications in anti-reflection coatings and optoelectronic components.

Authors contributions HMR: Methodology, Formal analysis, Investigation, Writing—Review and Editing. NSD: Investigation, Writing—Review and Editing. EAAE: Methodology, Formal analysis, Investigation. NHE: Conceptualization, Methodology, Writing—Review and Editing. ANA: Investigation, Writing—Review and Editing. MOF: Investigation, Writing—Review and Editing.

Data availability The data that support the findings of this study are available on request from the corresponding author. The data are not publicly available due to privacy or ethical restrictions.

Declarations

Conflict of interest The authors declare that they have no known competing financial interests or personal relationships that could have appeared to influence the work reported in this paper.

Ethical approval This research did not contain any studies involving animal or human participants, nor did it take place in any private or protected areas hence no specific permissions were required.

References

Abdelghany, A., et al.: Effect of gamma-irradiation on (PEO/PVP)/Au nanocomposite: materials for electrochemical and optical applications. Mater. Des. **97**, 532–543 (2016)

Abdelrazek, E.M., et al.: Structural, optical, morphological and thermal properties of PEO/PVP blend containing different concentrations of biosynthesized Au nanoparticles. J. Mater. Res. Technol. **7**(4), 419–431 (2018)

Abdul Nabi, M., et al.: Effect of nano ZnO on the optical properties of poly (vinyl chloride) films. Int. J. Polym. Sci. **2014**, 1–7 (2014)

Abutalib, M.M., Yahia, I.: Analysis of the linear/nonlinear optical properties of basic fuchsin dye/FTO films: controlling the laser power of red/green lasers. Optik **179**, 145–153 (2019)

Ahmed, R., et al.: Influence of Fe_2O_3@ reduced graphene oxide nanocomposite on the structural, morphological, and optical features of the polyvinyl alcohol films for optoelectronic applications. Phys. Scr. **98**(5), 055928 (2023)

Albalawi, H., et al.: Synthesis and characterization of sodium alginate/polyvinyl alcohol/zinc oxide/iron oxide nanocomposites for electrochemical applications. Polym. Compos. **44**(3), 1762–1771 (2023)

Alhagri, I.A., et al.: Enhanced structural, optical properties and antibacterial activity of PEO/CMC doped TiO_2 NPs for food packaging applications. Polymers **15**(2), 384 (2023)

Alsalmah, H.A., et al.: Hybrid GO/TiO_2 nanoparticles reinforced NaAlg/PVA blend: nanocomposites for high-performance energy storage devices. Polym. Adv. Technol. **34**(9), 2831–2840 (2023)

Aziz, S.B., et al.: Optical characteristics of polystyrene based solid polymer composites: effect of metallic copper powder. Int. J. Metals **2013**, 1–6 (2013)

Cha, J., et al.: Comparison to mechanical properties of epoxy nanocomposites reinforced by functionalized carbon nanotubes and graphene nanoplatelets. Compos. B Eng. **162**, 283–288 (2019)

Chatterjee, D.P., Pakhira, M., Nandi, A.K.: Fluorescence in "nonfluorescent" polymers. ACS Omega **5**(48), 30747–30766 (2020)

Dadashi, S., Poursalehi, R., Delavari, H.: Structural and optical properties of pure iron and iron oxide nanoparticles prepared via pulsed Nd: YAG laser ablation in liquid. Proc. Mater. Sci. **11**, 722–726 (2015)

Davachi, S.M., et al.: The effect of nanoperlite and its silane treatment on the crystallinity, rheological, optical, and surface properties of polypropylene/nanoperlite nanocomposite films. Compos. B Eng. **175**, 107088 (2019)

De Koninck, M., Poirier, S.-C., Marsan, B.: Cu x Co3− x O4 Used as bifunctional electrocatalyst: physicochemical properties and electrochemical characterization for the oxygen evolution reaction. J. Electrochem. Soc. **153**(11), 2103 (2006)

Ebnalwaled, A., Thabet, A.: Controlling the optical constants of PVC nanocomposite films for optoelectronic applications. Synth. Met. **220**, 374–383 (2016)

El Sayed, A., Morsi, W.J.J.O.M.S.: α-Fe ₂O3/(PVA+ PEG) nanocomposite films; synthesis, optical, and dielectric characterizations. J. Mater. Sci. **49**, 5378–5387 (2014)

El-Bana, M., et al.: Preparation and characterization of PbO/carboxymethyl cellulose/polyvinylpyrrolidone nanocomposite films. Polym. Compos. **39**(10), 3712–3725 (2018)

El-Naggar, A., et al.: Embedding of 50% PVA/50% PVP blend with Sn 0.75 M 0.25 S 2,(M = Y, Fe, Cr, V); structural and optical study. Appl. Phys. A **127**, 1–11 (2021)

El-Naggar, A., et al.: Effect of ZnO/(Co or Mn) ratios on the structure and optical spectroscopy parameters of PVA/PVP/PEG blended polymer. Opt. Mater. **128**, 112411 (2022a)

El-Naggar, A.M., et al.: Improvement of the optical characteristics of PVA/PVP blend with different concentrations of SnS2/Fe. J. Vinyl Addit. Technol. **28**(1), 82–93 (2022b)

El-Naggar, A., et al.: Effect of MnS/ZnS nanocomposite on the structural, linear and nonlinear optical properties of PVA/CMC blended polymer. Opt. Mater. **128**, 112379 (2022c)

El-Naggar, A., et al.: Impact of loading PVA/CMC/PVP blend with CdS0.9M0.1 non-stoichiometrically doped by transition metals (M). Opt. Mater. **133**, 113085 (2022d)

El-Naggar, A., et al.: Structural, dielectric, linear and nonlinear optical parameters of Zn0.9Cu0.1S filled PVA/CMC/PEG blends. Opt. Quant. Electron. **55**(9), 790 (2023)

El-Sayed, S., et al.: DSC, TGA and dielectric properties of carboxymethyl cellulose/polyvinyl alcohol blends. Physica B **406**(21), 4068–4076 (2011)

Flores-Lasluisa, J.X., et al.: Copper-doped cobalt spinel electrocatalysts supported on activated carbon for hydrogen evolution reaction. Materials **12**(8), 1302 (2019)

Gupta, B., Agarwal, R., SarwarAlam, M.: Preparation and characterization of polyvinyl alcohol-polyethylene oxide-carboxymethyl cellulose blend membranes. J. Appl. Polym. Sci. **127**(2), 1301–1308 (2013)

Heiba, Z.K., Mohamed, M.B.: Effect of annealed and Mg-doped nano ZnO on physical properties of PVA. J. Mol. Struct. **1181**, 507–517 (2019)

Heiba, Z.K., Mohamed, M.B.: Effect of gamma radiation on structural and optical parameters of Sm₂O₃: Mn/PVA nanocomposite film. Opt. Quant. Electron. **52**, 1–14 (2020)

Heiba, Z.K., et al.: Optical and electrical properties of quantum composite of polyvinyl alcohol matrix with CdSe quantum dots. Colloid Polym. Sci. **294**, 357–365 (2016)

Heiba, Z., Mohamed, M.B., Imam, N.: Fine-tune optical absorption and light emitting behavior of the CdS/PVA hybridized film nanocomposite. J. Mol. Struct. **1136**, 321–329 (2017)

Heiba, Z.K., et al.: Structural and optical properties of Cd1−x Mn x Fe₂O₄/PMMA nanocomposites. J. Inorgan. Organomet. Polym. Mater. **30**, 1898–1906 (2020)

Heiba, Z.K., et al.: The role of Cd0.9Mg0.1S nanofillers on the structural, optical, and dielectric properties of PVA/CMC polymeric blend. Chem. Phys. Lett. **770**, 138460 (2021)

Heiba, Z.K., et al.: Effect of Mo-doping on the structure, magnetic and optical characteristics of nano CuCo₂O₄. J. Mater. Res. Technol. **10**, 832–839 (2021)

Heiba, Z.K., Mohamed, M.B., Ahmed, S.I.: Exploring the physical properties of PVA/PEG polymeric material upon doping with nano gadolinium oxide. Alex. Eng. J. **61**(5), 3375–3383 (2022)

Hermans, P., Weidinger, A.: X-ray studies on the crystallinity of cellulose. J. Polym. Sci. **4**(2), 135–144 (1949)

Kara, H., Oylumluoglu, G., Coban, M.B.: Photoluminescence properties of a new Sm(III) complex/PMMA electrospun composite fibers. J. Clust. Sci. **31**, 701–708 (2020)

Kaverlavani, S.K., Moosavifard, S., Bakouei, A.: Designing graphene-wrapped nanoporous CuCo$_2$O$_4$ hollow spheres electrodes for high-performance asymmetric supercapacitors. J. Mater. Chem. A **5**(27), 14301–14309 (2017)

Khordad, R.: Absorbance of Iron nanoparticles dispersed in the ethylene glycol and n-propanol. Armen. J. Phys. **9**(3), 211–219 (2016)

Kumar, K., et al.: Electrical conduction mechanism in NaCl complexed PEO/PVP polymer blend electrolytes. J. Non-Cryst. Solids **358**(23), 3205–3211 (2012)

Li, L.J.M.: Tunable memristic characteristics based on graphene oxide charge-trap memory. Micromachines **10**(2), 151 (2019)

Liu, X., et al.: The CuCo$_2$O$_4$/CuO composite-based microspheres serve as a battery-type cathode material for highly capable hybrid supercapacitors. J. Alloys Compd. **894**, 162566 (2022)

Mohamed, M.B., Abdel-Kader, M.J.A.P.A.: Effect of excess oxygen content within different nano-oxide additives on the structural and optical properties of PVA/PEG blend. Appl. Phys. **125**, 1–11 (2019)

Mohamed, M.B., Heiba, Z.K., Imam, N.: Optical and thermogravimetric analysis of Zn$_{1-x}$CuxS/PVA nano-composite films. J. Mol. Struct. **1163**, 442–448 (2018)

Morsi, M., et al.: Effect of lithium titanate nanoparticles on the structural, optical, thermal and electrical properties of polyethylene oxide/carboxymethyl cellulose blend. J. Mater. Sci. Mater. Electron. **29**, 15912–15925 (2018)

Nofal, M.M., et al.: Polymer composites with 0.98 transparencies and small optical energy band gap using a promising green methodology: structural and optical properties. Polymers **13**(10), 1648 (2021)

Ragab, H., Ahmad, F., Radwan, S.N.: Change spectroscopic studies and optimization electrical properties of PVP/PEO doped copper phthalocyanines. Physica B **502**, 97–102 (2016)

Rajeh, A., Morsi, M., Elashmawi, I.: Enhancement of spectroscopic, thermal, electrical and morphological properties of polyethylene oxide/carboxymethyl cellulose blends: combined FT-IR/DFT. Vacuum **159**, 430–440 (2019)

Reddy, K.R., et al.: Enhanced photocatalytic activity of nanostructured titanium dioxide/polyaniline hybrid photocatalysts. Polyhedron **120**, 169–174 (2016)

Sharma, A., Aggarwal, S.: Optical investigation of soda lime glass with buried silver nanoparticles synthesised by ion implantation. J. Non-Cryst. Solids **485**, 57–65 (2018)

Sheha, E., et al.: Structure, dielectric and optical properties of p-type (PVA/CuI) nanocomposite polymer electrolyte for photovoltaic cells. Optik **123**(13), 1161–1166 (2012)

Soliman, T., Vshivkov, S.A.: Effect of Fe nanoparticles on the structure and optical properties of polyvinyl alcohol nanocomposite films. J. Non-Cryst. Solids **519**, 119452 (2019)

Soliman, T., et al.: Impact of Mn–Ni spinal ferrite nanoparticles on the structural, morphological, surface roughness, and optical parameters of polyvinyl alcohol for optoelectronic applications. Soft Matter **19**(40), 7753–7763 (2023)

Taha, T., Saleh, A.: Dynamic mechanical and optical characterization of PVC/fGO polymer nanocomposites. Appl. Phys. A **124**(9), 600 (2018)

Taha, T., et al.: Effect of NiO NPs doping on the structure and optical properties of PVC polymer films. Polym. Bull. **76**, 4769–4784 (2019)

Wang, Q., Chen, D., Zhang, D.: Electrospun porous CuCo$_2$O$_4$ nanowire network electrode for asymmetric supercapacitors. RSC Adv. **5**(117), 96448–96454 (2015)

Xiong, H.-M., Zhao, X., Chen, J.-S.: New polymer−inorganic nanocomposites: PEO−ZnO and PEO−ZnO−LiClO$_4$ films. J. Phys. Chem. B **105**(42), 10169–10174 (2001)